Soft Matter

PAPER

View Article Online
View Journal | View Issue

Cite this: Soft Matter, 2017, 13, 134

Drop morphologies on flexible fibers: influence of elastocapillary effects

Alban Sauret,†*[a] François Boulogne,†[b] Katarzyna Somszor,[bc] Emilie Dressaire[c] and Howard A. Stone[b]

Received 18th April 2016,
Accepted 8th November 2016

DOI: 10.1039/c6sm00921b

www.rsc.org/softmatter

Various materials are made of long thin fibers that are randomly oriented to form a complex network in which drops of wetting liquid tend to accumulate at the nodes. The capillary force exerted by the liquid can bend flexible fibers, which in turn influences the morphology adopted by the liquid. In this paper, we investigate through a model situation the role of the fiber flexibility on the shape of a small volume of liquid on a pair of crossed flexible fibers. We characterize the liquid morphologies as we vary the volume of liquid, the angle between the fibers, and the length of the fibers. The drop morphologies previously reported for rigid crossed fibers, *i.e.*, a drop, a column and a mixed morphology, are also observed on flexible crossed fibers with modified domains of existence. In addition, at small tilt angles between the fibers, a new behavior is observed: the fibers bend and collapse. Depending on the volume of liquid, a thin column with or without a drop is reported on the collapsed fibers. Our study suggests that the fiber flexibility adds a rich variety of behaviors that may be important for some applications.

1 Introduction

A capillary bridge between two spheres or two surfaces is known to exert a force that tends to keep the two solid bodies together.[1–3] For soft surfaces, the combination of the capillary force and the bending and/or stretching of the material leads to an elastocapillary equilibrium in which the elastic deformations of the substrate is related to the intensity of the capillary adhesion.[4,5] Elastocapillary effects are, for instance, responsible for the formation of bundles with flexible beams[6–8] or fibers,[9,10] the collapse of beams in MEMS applications[8,11–13] and in carbon nanotube[14] or in biological situations such as the wetting of feathers.[15]

Elastocapillary effects can be particularly important when considering thin elongated structures, such as fibers, whose length can be several orders of magnitude larger than their diameter; fibers are therefore prone to bend.[9,16–19] In addition, fibers, rigid or flexible, can be found in a variety of applications such as in wet hair,[6] in the textile industry,[20–22] in filters,[23,24] fog-harvesting nets[25–27] or insulation materials, including glass wool.[28,29] Therefore, many studies have considered the addition of liquid on an array of fibers through model systems that consist of a finite volume of wetting liquid deposited on a single or a pair of fibers.[30–32] These model situations allow investigation of the equilibrium shapes of the liquid and their influence on the drying process,[33,34] the capture of impacting drops,[35] the condensation of liquid[36] or the motion of drops along fibers.[37–41]

Past studies have considered the morphology adopted by a liquid drop deposited on a single fiber. For example, the addition of liquid on a single fiber can come from coating methods,[32] the condensation of liquid[36] or the impact of small droplets that are captured below an impact velocity threshold.[35,42,43] Once on the fiber, the drop can either adopt an axisymmetric (barrel shape) morphology or an asymmetric (clamshell) morphology where the drop sits on one side of the fibers.[31,44–47]

Considering rigid fibers, the presence of a second fiber close to the first one leads to different morphologies that depend on the contact angle of the liquid with the fiber, the inter-fiber distance, the tilt angle between them and the volume of liquid that is deposited. For instance, for two parallel fibers separated by a distance $2d$, the seminal work of Princen[30] shows that the liquid can either spread in a long liquid column, whose width is of the order of the fiber diameter if the fibers are close enough, or adopt a more compact drop shape when the inter-fiber distance is increased. More recently, three different possible morphologies have been reported for fibers of radius a randomly oriented, *i.e.*, tilted with an angle δ and separated by a minimum distance h. Depending on δ, $\tilde{h} = h/a$, and the dimensionless volume of liquid $\tilde{V} = V/a^3$, the liquid can be in a column shape, a mixed morphology state where a drop lies at

[a] Surface du Verre et Interfaces, UMR 125 CNRS/Saint-Gobain, 93303, Aubervilliers, France. E-mail: alban.sauret@saint-gobain.com
[b] Department of Mechanical and Aerospace Engineering, Princeton University, Princeton, New Jersey 08544, USA
[c] Department of Mechanical and Aerospace Engineering, New York University Tandon School of Engineering, Brooklyn, NY 11201, USA
† These authors contributed equally.

the end of a column, or a drop centered at the node, *i.e.*, the point where the two fibers are the closest.[28,48,49]

However, some fibrous materials, involve fibers that are very thin and long. Such high aspect ratio fibers are typically flexible. Therefore, the presence of liquid forming capillary bridges between fibers is susceptible to modify the liquid morphologies and the organization of the fibers in a randomly oriented array. Indeed, the presence of liquid can lead to the clustering of flexible structures as shown by Py *et al.*[16] who investigated the behavior of a model brush of parallel flexible fibers withdrawn from a liquid bath. To describe their experimental findings, the authors defined an elastocapillary lengthscale:[4,6]

$$\ell_{\mathrm{EC}} = \sqrt{\frac{EI}{\gamma a}}, \qquad (1)$$

where E is the Young's modulus of the fiber, $I = \pi a^4/4$ is the polar moment of inertia, a the radius and γ the liquid surface tension. The elastocapillary length can be derived from the balance between the capillary energy $\gamma a L_{\mathrm{fib}}$ and the bending energy EIL_{fib}/R^2 where R is the typical radius of curvature. This balances leads to $l_{\mathrm{EC}} = R$, and the elastocapillary length can be seen as a local radius of curvature of the fiber.

Because the capillary force and the elasticity of the fibers can lead to the deformation of the fibers,[50] different configurations have been investigated. In particular, Duprat *et al.* considered parallel fibers whose spacing and length are controlled and a known volume of wetting liquid is deposited.[17] Different morphologies were observed: a drop state, a column morphology or a mixed morphology. In addition, the presence of liquid was shown to bend the fibers and influence the final liquid morphology. In their configuration, the elastocapillary length is around $l_{\mathrm{EC}} \sim 55$ cm whereas the length of the fibers L_{fib} is typically a few centimeters. In such model experiments, although $L_{\mathrm{fib}} \ll l_{\mathrm{EC}}$, the effects of the flexibility can be observed experimentally and lead to the presence of new liquid morphologies.

However, the more general situation of tilted flexible fibers, encountered in arrays, has not been studied. The presence of liquid at a node is expected to introduce a capillary force and a torque that can modify the orientation of the fibers and lead to different morphologies.[51] However, no systematic experimental investigations has been reported to date. To study this situation, we consider two crossed fibers, clamped at one of their ends and free to move at the other, in contact at the node and tilted with an angle $\delta = [0,90]^\circ$. Using experiments, we then investigate the morphologies and the equilibrium orientations of the fibers while varying the imposed initial tilt angle δ and the volume of liquid V deposited on the fibers. We highlight the presence of two new morphologies compared to the situation of crossed rigid fibers: a column collapsed state and a drop-collapsed state. In this paper, we first present the experimental method in Section 2. In Section 3, we describe the new morphologies and a morphology diagram in the $(\delta,\tilde{V})$ space is reported. We then rationalize our results to explain these new morphologies. Finally, we highlight in section 4 that hysteresis effects can be large in such systems owing to capillary effects.

2 Experimental protocol

In our experiments, the fibers consist of thin capillary cylindrical tubes (purchased from VitroCom) of outer diameter $2a = 250$ μm and inner diameter $2b = 150$ μm. We seal the end of the tube with a small amount of epoxy glue so that no liquid can flow into the capillary tube. We have measured the bending modulus of these fibers using their deflection under their own weight and obtained $B = 8.1 \times 10^{-6}$ Pa m^4, in agreement with the estimated theoretical value $B = EI = \pi E(a^4 - b^4)/4$, where I is the polar moment of inertia of the cross section of the fiber. The weight per unit length is $\rho_l = 3.5 \times 10^{-5}$ kg m^{-1}. Therefore, the value of the elastocapillary length in our system is $l_{\mathrm{EC}} \simeq 1.8$ m, which is of the same order of magnitude as the one of previous experiments investigating elastocapillary effects between parallel fibers.[17] In this paper, we study a system in which the typical drop size $V^{1/3}$ is much smaller than the elastocapillary length, *i.e.*, $V^{1/3} \ll l_{\mathrm{EC}}$. As a consequence the fibers cannot bend on the lengthscale of the drop. Roman and Bico studied the opposite limit and they observed that a soft fiber coils around a liquid drop.[4]

One extremity of each fiber is clamped on a (x,y,z) microcontroller linear stage (PT3, Thorlabs). Fibers cross at the node. One of the controllers is allowed to rotate around the node with a rotation mount (PR01, Thorlabs) to accurately tune the angle δ between the fibers. We denote L_{fib} the total length of a fiber and L_{free} the distance between the node and the tip of the fiber (Fig. 1). In all experiments presented in this paper, the lengths L_{fib} and L_{free} are identical for both fibers. The vertical deflection of fibers due to their own weight and the weight of the drop is limited to 3 mm for the largest fiber length ($L_{\mathrm{fib}} = 90$ mm) and the largest drop volume ($V = 8$ μl). We should emphasize that we could not use longer fibers since gravity effects will then become too important.

Before each experiment, the horizontal positions of the microcontrollers are adjusted to ensure that L_{free} remains constant while varying the tilt angle δ. The vertical positions of the linear microcontrollers are then adjusted to bring the fibers into contact. In all the experiments, we use a perfectly wetting fluid (5 cSt silicone oil, contact angle $\theta = 0^\circ$, density $\rho = 918$ kg m^{-3}, surface tension $\gamma = 19.7$ mN m^{-1}). A volume $V \in [1,8]$ μl is initially dispensed with a micropipette (Eppendorf, Research Plus) at the node of the fibers. Because the fibers are flexible and bend under capillary effects, the apparent angle between

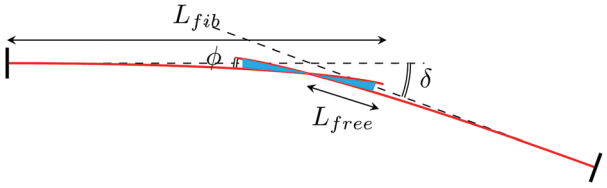

Fig. 1 Schematic of the experimental setup showing the wetting liquid and the tilted fibers. Both fibers are clamped at one end and free at the other end so that they can bend owing to a capillary force. Experimentally, we impose a tilt angle δ and the elasticity of the fibers leads to a new angle ϕ.

the fiber ϕ can be smaller than the tilt angle without liquid δ as illustrated by the schematic in Fig. 1. In our experiments, we assume that the gravitational effects on the liquid bridge can be neglected. Indeed, the capillary length, $l_c = \sqrt{\gamma/(\rho g)} \simeq 1.5$ mm, is larger than the typical height H of the liquid. In addition, we neglect gravitational effects on the fibers because, in the absence of liquid, the fibers do not bend significantly under their own weight with the chosen length L_{fib}, as noted above.

We start the experiment at a large tilt angle between the fibers (typically $\delta = 60^\circ$) and the angle is reduced to the desired value. The imposed tilt angle δ is directly measured on the rotation microcontroller with an uncertainty of about 0.5°. We wait for a few minutes to ensure that the final steady liquid morphology is reached and record images from the top and from the side using Nikon cameras (D5100 and D7100) and 105 mm macro lenses. The induced angle ϕ is measured using the top view images (corresponding to the schematic in Fig. 1) by image processing with an uncertainty of about 0.5°. When a steady morphology has been reached and the images recorded, we increase or decrease the angle δ between the fibers and ensure that L_{free} remains constant and wait until a new steady state is reached. Using this method, we explore the influence of the volume of liquid, the tilt angle δ between the fibers, the total length L_{fib} and the free end L_{free} of the fibers on the final morphology.

3 Morphologies and transitions

3.1 Morphology diagram

Our experimental observations highlight that the three liquid morphologies observed on rigid crossing fibers are recovered with flexible fibers as illustrated in Fig. 2(a)–(c):[28] (i) the drop state for large angles (typically $\delta > 35^\circ$) where the liquid collects at the node of the fiber and forms a single hemispherical drop, (ii) a mixed morphology when the tilt angle is decreased and in which the liquid partially spreads into a column but a drop remains located on one side of the column (note that the side of the column where the drop is located is random and induced by perturbations present in the surrounding environment or introduced when changing the tilt angle) and (iii) a column state at small angles and small volume where the liquid spreads between the fibers and where the height of the column is typically comparable to the fiber diameter.

Considering crossed flexible fibers that are clamped on one end and free to move at their other end leads to two previously unreported morphologies, shown in Fig. 2(d) and (e). This response is indeed caused by the flexibility of the crossed fibers. The presence of the wetting liquid located at the node, *i.e.*, the point where the two fibers cross, results in capillary forces that tend to pull on fibers and cause them to deflect inwards. This elastocapillary effect decreases the local distance between the fibers and the liquid can thus continue to spread spontaneously along the fibers. The magnitude of the capillary force increases, further bending the fibers, until they stick to one another, *i.e.*, collapse, and the liquid can form a thin long column. The interfacial and bending energies therefore lead to the observed collapsed morphology reported in Fig. 2(d). Finally, if more liquid is added to the system, the thin column keeps spreading until it reaches the full length of the sticking region,

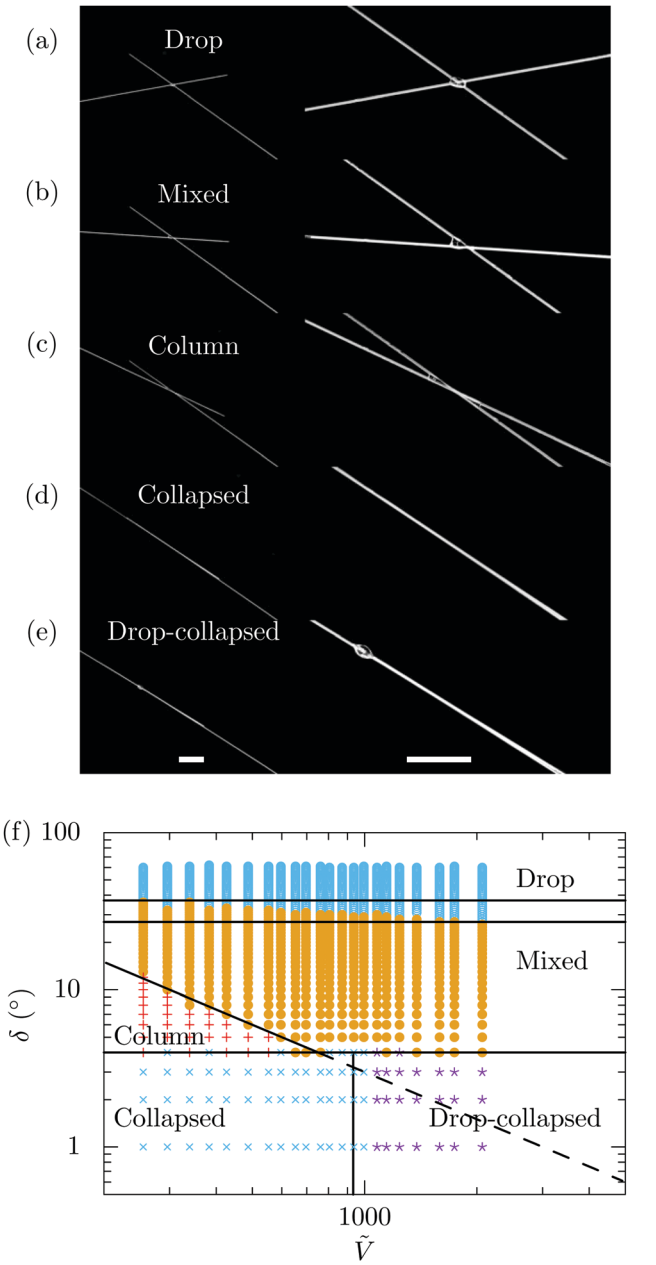

Fig. 2 Top views of the five different morphologies observed between two flexible fibers crossing as the angle δ is decreased: (a) drop, (b) mixed and (c) column morphology, as observed for rigid fibers. The flexibility of the fibers introduces two new morphologies at small tilt angle, the (d) collapsed and (e) drop-collapsed morphologies. The right column shows zoomed views of the morphologies. The scale bars represent 1 cm. (f) Morphology diagram in the (V/a^3,δ) space for fibers of radius a = 125 μm showing the drop (blue circles), mixed (yellow circles), column (red crosses), collapsed (blue crosses) and drop-collapsed (purple stars) morphologies. The solid lines indicate the approximate transitions between the different regions. The dashed line represents the mixed-column transition that cannot be observed for flexible fibers. In this figure, L_{free} = 18.6 mm and L_{fib} = 86.7 mm.

$2L_{free}$, and a drop grows at one end of the column. The results in the drop-collapsed morphology are shown in Fig. 2(e).

We experimentally characterize the regions of existence of the five different morphologies observed for crossed flexible fibers having a constant total length L_{fib} and a free length L_{free}. We perform systematic experiments varying the liquid volume $\tilde{V} = V/a^3$ and the tilt angle δ, and report our results in a ($\tilde{V}$, δ) morphology diagram in Fig. 2(f). Both the collapsed and drop-collapsed morphologies are observed below a tilt angle δ typically smaller than 5° for the fibers considered. Above this angle, we recover the morphology diagram of the rigid fibers as the capillary force is not sufficient to significantly bend the fibers at large tilt angle δ. Indeed, the column/mixed morphology transition described by Sauret *et al.*[28] for rigid fibers satisfactorily captures the column/mixed morphology transition for flexible fibers as reported in Fig. 2(f). In addition, the column/drop and mixed/drop morphology transitions are also observed for a critical angle $\delta = 35 \pm 5°$, as reported for rigid fibers. The key difference is therefore that, below a critical angle, the classical column morphology is not observed but instead the fibers stick to one another in a collapsed state. In addition, in this regime of small angles, we observe a state of partial spreading for sufficiently large volume of liquid: a smaller drop remains at the edge of the collapsed region.

3.2 Transitions at large angles: drop, mixed and column morphologies

If the fibers are sufficiently rigid or the capillary force too weak to bend the fibers, the local angle at the node must be equal to the global tilt angle, that is $\delta = \phi$. We measure the local angle ϕ as a function of the global angle δ in our system. The results indicate that the capillary force is not sufficient to significantly bend the fibers for $\delta > 4°$ for the fibers used in our experiments, which is the angle at which the collapse transition occurs. Note that the value at which the bending of the fibers becomes important depends on the flexibility of the fibers and thus on the elastocapillary length compared to the fibers length. Therefore, the transition between the different regimes can be described by the model developed for rigid fibers, and described in previous publications.[28,48]

3.3 Transitions to the collapsed states

The transition between the column or mixed morphology (Fig. 2(b) and (c)) and the collapsed state (Fig. 2(d) and (e)) is more complex. The bending and collapse of the fibers result from an elastocapillary equilibrium. To rationalize these results, despite the complex shape of the liquid column, we can estimate the energy associated with the bending of a fiber in the collapsed state and the energy associated to the capillary bridge induced by the liquid column in the collapsed state. Different simplified situations have considered this elastocapillary equilibrium between parallel sheets or fibers.[6,16,17] We denote d the distance over which the fiber needs to be deflected for the fibers to stick to one another along L_{free}. Using geometrical considerations, we have

$$\sin\delta = \frac{d}{L_{free}}. \quad (2)$$

Because the collapse happens in the limit of small angles, $\delta \ll 1$, we can simplify (2) to $d = \delta L_{free}$. Using the same notations as Bico *et al.*,[6] we define the length of the wet segment of the fiber as $L_{wet} = L_{fib} - L_{dry}$, where L_{fib} and L_{dry} are the total length of a fiber and the dry part, respectively. The bending energy E_c associated to the deformation of the two fibers that coalesce at a distance L_{dry} is

$$E_c \simeq \frac{6Bd^2}{{L_{dry}}^3}. \quad (3)$$

To simplify, we consider the capillary force induced by a liquid column when the fibers are in the collapsed state and therefore the fibers are parallel. In this situation, the liquid column has a constant cross-sectional area $A \simeq \pi a^2$ on the entire free length $L_{wet} = 2(L_{fib} - L_{dry})$. Therefore, the energy associated to the capillary force is

$$E_s \sim -2\gamma a(\pi - 2)(L_{fib} - L_{dry}), \quad (4)$$

where we assume that we can neglect the contribution of the terminal menisci and that the column is flat. This equation leads to an expression for L_{dry}:[17]

$$L_{dry} \simeq \left(\frac{9Bd^2}{\gamma a(\pi - 2)}\right)^{1/4}. \quad (5)$$

Using eqn (2), and considering that the fibers collapse when $L_{wet} = 2L_{free} = 2(L_{fib} - L_{dry})$ we obtain the following estimate for the tilt angle δ

$$\delta \simeq \frac{(L_{fib} - L_{free})^2}{L_{free}}\sqrt{\frac{\gamma a(\pi - 2)}{9B}}. \quad (6)$$

Introducing the elastocapillary length l_{EC} defined in eqn (1), and the ratio between the free length and the total length of the fiber $\alpha = L_{free}/L_{fib}$, this expression can be rewritten as:

$$\delta \simeq \frac{L_{fib}}{l_{EC}}\frac{(1-\alpha)^2}{\alpha}\sqrt{\frac{(\pi - 2)}{9}}, \quad (7)$$

which shows that increasing the total length of the fiber or decreasing the elastocapillary length leads to a collapsed state for larger tilt angle. This expression is valid for moderately flexible fibers, typically for $L_{fib} < l_{EC}$.

The experimental results obtained by varying the total length of the fiber L_{fib} are in qualitative agreement with this expression as illustrated in Fig. 3: the longer the fibers, the easier the collapse. Note that the order of magnitude estimate given here could be refined by considering the exact length and shape of the column for a given volume. As a result, the energy associated with the capillary bridge between the fibers could be calculated between two crossed fibers.[28] However, such calculations would require to know the inter-fibers distance, which is modified by the elastocapillary equilibrium even before the collapsed state.

With typical experimental values, $L_{fib} = 87$ mm, $L_{free} = 18.5$ mm, $B = EI = 8.1 \times 10^{-6}$ Pa m^4, $a = 125$ mm, $\gamma = 19.7$ mN m^{-1}, from (7) we obtain $\delta \sim 3°$. This result is satisfactorily close to the observed value and shows that elastocapillary effects are indeed

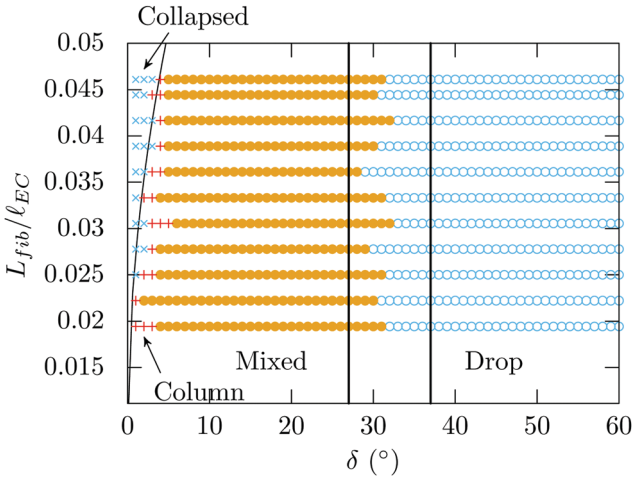

Fig. 3 Morphologies observed for fibers of radius a = 125 μm, l_{EC} = 1.8 m and varying L_{fib}/l_{EC}. L_{free}= 14 mm, the volume $\tilde{V}$ = 768 and a = 125 μm are constant. The black solid curve represents eqn (7). The vertical black lines show the drop-mixed transition represented in Fig. 2(f).

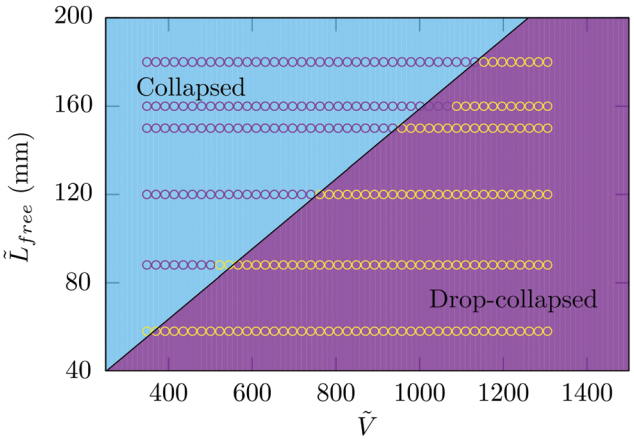

Fig. 4 Threshold value of the volume of liquid delimiting the collapsed and drop-collapsed states for varying length of the free end of the fiber $\tilde{L}_{free}$ = L_{free}/a. The continuous black line is defined by eqn (8) and the experimental parameters kept constant are a = 125 μm and L_{fib} = 110 mm.

responsible for the collapse of the fibers at sufficiently small angle. However, we shall see that because of our assumption of a flat shape, the transition between the column or mixed morphology and the collapsed state is only an order of magnitude. In addition, because of the shape of the capillary bridge in the column and the collapsed morphologies, the angle necessary for the fibers to release from the sticking state will be larger than the angle for the fibers to collapse. Indeed, flexible fibers that collapse owing to capillary effects present a strong hysteresis as described in Section 4.

3.4 Transition between collapsed and drop-collapsed morphologies

We now turn to the transition between the collapsed and drop-collapsed morphologies. Similarly to the situations described for parallel fibers, when the fibers collapse, the liquid shape can be assumed to be a long straight column with a cross-sectional area $A \simeq \pi a^2$.[17] Because the liquid can spread over a distance L_{free} on each side of the node, the critical volume that describes the transition between collapsed and drop-collapsed morphologies is $V_c = 2\pi a^2 L_{free}$ leading to the critical dimensionless volume

$$\tilde{V}_c = \frac{2\pi L_{free}}{a}. \quad (8)$$

This expression is in agreement with our experimental observation reported on the morphology diagram in Fig. 2(f). In addition, we perform systematic experiments varying the free length of the fiber beyond the node, L_{free}. The volume of liquid at the transition is thus measured and the results shown in Fig. 4 are well captured by eqn (8). Beyond the threshold value V_c, adding more liquid leads to the formation of a liquid drop at one end of the thin column.

4 Hysteresis

The morphology diagram (Fig. 2(f)) presented in this article is established by starting at large tilt angle δ and then decreasing the angle for each dimensionless volume of liquid $\tilde{V}$ considered. However, we also perform experiments considering the opposite situation: we start with collapsed fibers and incrementally increase the tilt angle until the collapsed to column/mixed morphology transition occurs (Fig. 2(d) and (e) then Fig. 2(b) and (c)). We observe that the critical tilt angle δ_r at which the fibers separate is much larger than the angle δ_c at which the fibers collapse. We have reported these hysteretic measurements in Fig. 5 for different volumes of liquid.

We observe that the amount of liquid seems to have no influence on the coalescence and separation angles in the range of volumes considered. Indeed, when the fibers are collapsed, the liquid spreads along a thin liquid column and, the volume considered is sufficiently large for the liquid to reach the free ends of the fibers. Therefore, the energy associated with the capillary force can be assumed constant as well as the bending energy that is necessary for the fibers to be released at δ_r.

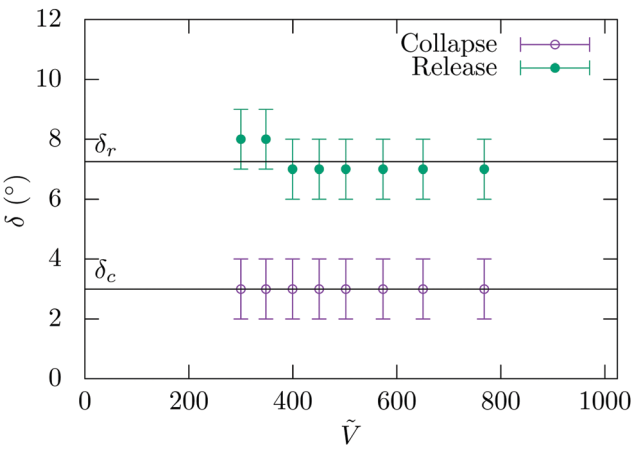

Fig. 5 Critical angles for the fibers to collapse δ_c (hollow circles) when decreasing the tilt angle and to separate δ_r (filled circles) when the tilt angle is increased for varying volume of liquid V. The fibers have a radius a = 125 μm, a total length L_{fib} = 87 mm and a free length L_{free} = 18.6 mm.

Finally, we explore the effects of the free length L_{free} on the critical angle δ_r for the separation of collapsed fibers. Indeed, the capillary force associated to the wetting of parallel fibers on a distance L_{free} is $E_s = -2\gamma a(\pi - 2)L_{free}$. Therefore, increasing the free length of the fibers qualitatively leads to an increase of the adhesion force, increasing the critical angle for the separation of the collapsed fibers. This hysteresis effect between the column/mixed and collapsed morphologies may modify significantly the lower part of the morphology diagram shown in Fig. 2(f).

5 Conclusion

In this paper, we have experimentally illustrated that flexible crossed fibers share similar morphologies to the system of rigid fibers. In particular, at large tilt angle δ, the three morphologies obtained for rigid crossed fibers are recovered. However, when decreasing the tilt angle, the energy required to collapse the fibers decreases while the capillary force increases. The capillary force first leads to a larger deflection of the fibers, namely the tilt angle between the fibers is locally decreased ($\phi < \delta$) slightly modifying the column to mixed morphology transition. In addition, we have reported two new morphologies at small tilt angle δ: a column collapsed and a drop-collapsed morphology where the fibers are locally parallel. The transition between these two morphologies can be explained by considering the maximum amount of liquid that can spread into a long thin column around collapsed fibers. The transition between the column or mixed morphology and the collapsed morphologies can be captured by considering an elastocapillary equilibrium, as observed for parallel lamellae or fibers. We also observe a strong hysteresis in the system between the column/mixed and collapsed morphologies. The experiments in this study are performed in the regime where $L_{fib}/l_{EC} \ll 1$. Future works will need to investigate the situation $L_{fib}/l_{EC} > 1$ where the effects of the flexibility are expected to be even greater. For instance, the influence of the flexibility of the fibers can be especially important in systems where the porosity of the fiber network needs to be large as capillary effects will tend to align fibers and form large clusters.[6–8]

Acknowledgements

The work of AS is partially supported by a CNRS PICS grant no. 07242. KS and ED acknowledge financial support from NYU Tandon School of Engineering's Undergraduate Summer Research Program. FB acknowledges that the research leading to these results partially received funding from the People Programme (Marie Curie Actions) of the European Union's Seventh Framework Programme (FP7/2007–2013) under REA grant agreement 623541.

References

1 L. R. Fisher and J. N. Israelachvili, *J. Colloid Interface Sci.*, 1981, **80**, 528–541.
2 C. H. Mastrangelo and C. H. Hsu, *Systems*, 1993, **2**, 33–43.
3 C. D. Willett, M. J. Adams, S. A. Johnson and J. Seville, *Langmuir*, 2000, 9396–9405.
4 B. Roman and J. Bico, *J. Phys.: Condens. Matter*, 2010, **22**, 493101.
5 J. L. Liu and X. Q. Feng, *Acta Mech. Sin.*, 2012, 928–940.
6 J. Bico, B. Roman, L. Moulin and A. Boudaoud, *Nature*, 2004, **432**, 690.
7 K. Singh, J. R. Lister and D. Vella, *J. Fluid Mech.*, 2014, **745**, 621–646.
8 B. Pokroy, S. H. Kang, L. Mahadevan and J. Aizenberg, *Science*, 2009, **323**, 237–240.
9 A. Boudaoud, J. Bico and B. Roman, *Phys. Rev. E: Stat., Nonlinear, Soft Matter Phys.*, 2007, **76**, 060102.
10 Q. Wang, B. Su, H. Liu and L. Jiang, *Adv. Mater.*, 2014, **26**, 4889–4894.
11 D. Chandra, S. Yang and A. A. Soshinsky, *ACS Appl. Mater. Interfaces*, 2009, **1**, 1698–1704.
12 D. Chandra and S. Yang, *Acc. Chem. Res.*, 2010, **43**, 1080–1091.
13 M. De Volder and A. J. Hart, *Angew. Chem., Int. Ed.*, 2013, **52**, 2412–2425.
14 N. Chakrapani, B. Wei and A. Carrillo, *Proc. Natl. Acad. Sci. U. S. A.*, 2004, **101**, 4009–4012.
15 R. Clark, *Environ. Pollut., Ser. A*, 1984, **33**, 1–22.
16 C. Py, R. Bastien, J. Bico, B. Roman and A. Boudaoud, *EPL*, 2007, **77**, 44005.
17 C. Duprat, S. Protiere, A. Y. Beebe and H. A. Stone, *Nature*, 2012, **482**, 510–513.
18 H. Elettro, S. Neukirch, F. Vollrath and A. Antkowiak, *Proc. Natl. Acad. Sci. U. S. A.*, 2016, 201602451.
19 R. D. Schulman, A. Porat, K. Charlesworth, A. Fortais, T. Salez, E. Raphaël and K. Dalnoki-Veress, 2016, arXiv preprint arXiv:1607.05990.
20 F. W. Minor, A. M. Schwartz, E. Wulkow and L. C. Buckles, *Text. Res. J.*, 1959, **29**, 931–939.
21 B. Miller, A. B. Coe and P. N. Ramachandran, *Text. Res. J.*, 1967, **37**, 919–924.
22 L. Eadie and T. K. Ghosh, *J. R. Soc., Interface*, 2011, rsif20100487.
23 B. J. Mullins, I. E. Agranovski, R. D. Braddock and C. M. Ho, *J. Colloid Interface Sci.*, 2004, **269**, 449–458.
24 P. Contal, J. Simao, D. Thomas, T. Frising and S. Callé, *J. Aerosol Sci.*, 2004, **35**, 263–278.
25 J. Ju, H. Bai, Y. Zheng, T. Zhao, R. Fang and L. Jiang, *Nat. Commun.*, 2012, **3**, 1247.
26 K. C. Park, S. S. Chhatre, S. Srinivasan and R. E. Cohen, *Langmuir*, 2013, **29**, 13269–13277.
27 R. LeBoeuf and E. de la Jara, *Water Int.*, 2014, **39**, 431–450.
28 A. Sauret, F. Boulogne, B. Soh, E. Dressaire and H. A. Stone, *Eur. Phys. J. E: Soft Matter Biol. Phys.*, 2015, **38**, 62.
29 P. B. Bintein, *Dynamiques de Gouttes Funambules: Applications à la Fabrication de Laine de Verre*, PhD thesis, Université Pierre et Marie Curie, 2015.
30 H. Princen, *J. Colloid Interface Sci.*, 1970, **34**, 171–184.
31 B. Carroll, *Langmuir*, 1986, **2**, 248–250.
32 D. Quéré, *Annu. Rev. Fluid Mech.*, 1999, **31**, 347–384.

33 B. Sutter, D. Bémer, J.-C. Appert-Collin, D. Thomas and N. Midoux, *Aerosol Sci. Technol.*, 2010, **44**, 395–404.
34 F. Boulogne, A. Sauret, B. Soh, E. Dressaire and H. A. Stone, *Langmuir*, 2015, **31**, 3094–3100.
35 E. Lorenceau, C. Clanet and D. Quéré, *J. Colloid Interface Sci.*, 2004, **279**, 192–197.
36 K. Zhang, F. Liu, A. J. Williams, X. Qu, J. J. Feng and C. H. Chen, *Phys. Rev. Lett.*, 2015, **115**, 074502.
37 T. Gilet, D. Terwagne and N. Vandewalle, *Appl. Phys. Lett.*, 2009, **95**, 014106.
38 T. Gilet, D. Terwagne and N. Vandewalle, *Eur. Phys. J. E: Soft Matter Biol. Phys.*, 2010, **31**, 253–262.
39 F. Boulogne, L. Pauchard and F. Giorgiutti-Dauphiné, *J. Fluid Mech.*, 2012, **704**, 232–250.
40 F. Weyer, M. Lismont, L. Dreesen and N. Vandewalle, *Soft matter*, 2015, **11**, 7086–7091.
41 A. Bick, F. Boulogne, A. Sauret and H. A. Stone, *Appl. Phys. Lett.*, 2015, **107**, 181604.
42 K. Piroird, C. Clanet, E. Lorenceau and D. Quéré, *J. Colloid Interface Sci.*, 2010, **334**, 70–74.
43 E. Dressaire, A. Sauret, F. Boulogne and H. A. Stone, *Soft Matter*, 2016, **12**, 200–208.
44 B. Carroll, *J. Colloid Interface Sci.*, 1976, **57**, 488–495.
45 G. McHale, M. I. Newton and B. J. Carroll, *Oil Gas Sci. Technol.*, 2001, **56**, 47–54.
46 G. McHale and M. I. Newton, *Colloids Surf., A*, 2002, **206**, 79–86.
47 X. F. Wu, M. Yu, Z. Zhou, A. Bedarkar and Y. Zhao, *Appl. Surf. Sci.*, 2014, **294**, 49–57.
48 A. Sauret, A. D. Bick, C. Duprat and H. A. Stone, *EPL*, 2014, **105**, 56006.
49 A. Sauret, F. Boulogne, D. Cébron, E. Dressaire and H. A. Stone, *Soft Matter*, 2015, **11**, 4034–4040.
50 M. Soleimani, R. J. Hill and T. G. M. van de Ven, *Langmuir*, 2015, **31**, 8328–8334.
51 J. O. Claussen, *Elasticity and Morphology of Wet Fibers*, PhD thesis, University of Göttingen, 2011.

